Hindawi
Shock and Vibration
Volume 2020, Article ID 8826272, 13 pages
https://doi.org/10.1155/2020/8826272

Research Article

Seismic Performance Analysis of Self-Centering Concentrically Braced Steel Frame Structures

Ergang Xiong,[1] **Kun Zu**,[1] **and Qian Zhang**[2]

[1]*Chang'an University, Xi'an, Shaanxi Province, China*
[2]*Xi'an Eurasia University, Xi'an, Shaanxi Province, China*

Correspondence should be addressed to Ergang Xiong; xerg@chd.edu.cn

Received 2 May 2020; Revised 27 May 2020; Accepted 9 June 2020; Published 9 September 2020

Academic Editor: Xing Ma

To study the seismic performance of self-centering concentrically braced frame (SC-CBF) structure, the static elastoplastic analysis, low-cycle repeated loading analysis, and elastoplastic time-history analysis were conducted for a four-story SC-CBF structure, compared with the traditionally concentrically braced frame (CBF) structure. The influences of different GAP stiffnesses and cross-sectional areas of prestressed tendon were investigated on the self-centering and seismic performance of the SC-CBF structure. The results show that the SC-CBF structure has a strong lateral resistance, a small base shear under earthquake action, and a slight residual drift after unloading. The SC-CBF structure has a better ductility than the CBF structure. The displacement of the SC-CBF structure under the action of rare and extremely rare earthquakes is large, and the structure can dissipate more energy; the interstory drift is large, but the residual drift is small, exhibiting its ideal seismic and self-centering performance. However, the mechanical behavior of prestressed tendons is significantly affected by the stiffness of the GAP. The mechanical and seismic performances of the overall structure are slightly affected by the stiffness of the GAP, but the cross-sectional area of the prestressed tendons has a remarkable influence on the overall performance of the structure.

1. Introduction

The steel frame structure has so many significant advantages such as good seismic performance, lightweight, and short construction period, so it is widely used in architecture structures nowadays. However, the steel frame structure would undergo serious damages under the action of earthquake according to the earthquake disaster analysis. Meanwhile, the structure has a large residual drift after earthquake and cannot be desirably repaired [1, 2]. At present, on the basis of the seismic design idea that the structure would not collapse under major earthquakes, be repairable under moderate earthquakes, and have no damages under minor earthquakes specified in Chinese code for seismic design of buildings (GB 50011-2010) [3], the earthquake-resilient structures can recover structural function as soon as possible with some reparations after earthquake, which could well achieve the seismic resilient design goal [4–6].

As a common form of earthquake-resilient structures, the self-centering structure can effectively diminish the residual drift and recover the structures' normal function under the action of earthquake. One of the feasible ways to realize the self-centering function is to apply prestress in the steel frame structure [7]. The concentrically braced steel frame (CBF) structure can effectively improve the lateral resistance and seismic performance for the structure, thus considered to be an ideal lateral force resisting system [8]. However, the column base of the CBF structure is rigidly fixed with the foundation, which enables the structure to have a large lateral stiffness and a small lateral displacement under the horizontal earthquake action. But the structures' displacement ductility is limited, and the restrained bracings are prone to buckling, resulting in a large residual drift and technical difficulties in repairing structure after the earthquake. Ricles et al. [9] proposed the self-centering steel frame by setting horizontal prestressed steel cable in the beam and then connecting with the column, and thus, part of the shear

force is carried by the energy dissipating member. The prestressed steel cable can reduce the structure's residual deformation and provide the recovery for the structure. Due to the limitations of the CBF structure, Sause et al. [10, 11] applied the self-centering thought on the CBF structure and put forward a kind of self-centering concentrically braced steel frame structure (SC-CBF). To realize the design performance, the SC-CBF structure releases the column base and permits the column to decompress and uplift; the self-centering function can be realized by setting prestressed tendon at the column axis. Roke et al. [12] found that the SC-CBF structure can achieve the expected lateral deformation and self-centering performance by time-history analysis, considering three different prestressed tendon positions. And in the later study, it was concluded that SC-CBF structure can effectively control the structure's residual drift under the earthquake action, providing a better safety and overall deformation performance [13].

This paper aims to explore the seismic performance of self-centering concentrically braced frame (SC-CBF) structure; the static elastoplastic analysis, low-cycle repeated loading analysis, and elastoplastic time-history analysis are conducted for a four-story SC-CBF structure, compared with the traditionally concentrically braced frame (CBF) structure. Moreover, the effects of different GAP element stiffnesses and cross-sectional areas of prestressed tendon are investigated on the self-centering and seismic performance of the SC-CBF structure.

2. Working Principle and Analysis Modeling

2.1. Working Principle. The self-centering structure is originated from the application of sway column. The column can rotate freely under the horizontal force, so as to reduce the damage of members by relaxing the constraint between the foundation and structure. Based on this, it is possible to put forward the self-centering concentrically braced frame via relaxing the column base of the steel frame structure. Figure 1 shows the mechanical model of SC-CBF structure; the structural forms of SC-CBF and CBF are similar, but the SC-CBF structure has relaxed the connection of foundation and column base, which allows the column base to decompress and uplift under the action of horizontal force. Meanwhile, prestressed tendon is set vertically in the middle of the structure to provide restoring force for the structure rotation. In order to increase the structural energy dissipating capacity, the friction devices are set between the self-centering column and the gravity column or the energy dissipating element is added in the lifting part of the column base, which is different from the site of energy dissipating members for the CBF structure.

Figure 2(a) and 2(b) shows the rocking behavior of the SC-CBF structure. Figure 2 reflects the deformation and rocking of the structure under the action of moderate and rare horizontal earthquakes, respectively. SC-CBF only undergoes elastic deformation when the structure suffers a small horizontal force; the structure's column and foundation are fixed, and the top displacement is small, which is similar to the CBF structure. However, when the horizontal

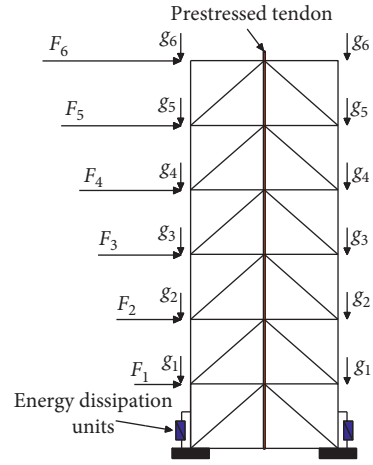

Figure 1: Mechanical model of the SC-CBF structure.

force is large enough, the column base and foundation would be separated, the column base is lifted, and the top displacement of the column increases the rigid body rotations of the structure. The sway change in the structure is exhibited, while the left and right column bases are lifted in Figure 2(b).

2.2. Parameters of SC-CBF Structure. The SC-CBF structure is designed as an example according to load code for building structures (GB 50009-2012) [14] and performance-based SC-CBF structure design method [15]; the floor and roof dead loads are 3.5 kN/m^2, the live load for the floor is 2.0 kN/m^2, and the snow load is 0.35 kN/m^2. The welded H-shaped sections are selected for both beams, columns, and bracings. Material type is defined as Q235 whose yield strength is 235 MPa. The members' size of the structure is shown in Table 1. This SC-CBF structure has four stories. The first story height is 4.5 m, and the other story height is 3 m. The seismic fortification intensity is 8 degree, the site condition is class II, and the design earthquake classification is the 2nd group. The floor plan and elevation of the structure are shown in Figures 3 and 4, respectively.

2.3. Structural Finite Element Model. The finite element planar model of the SC-CBF structure was established by the software OpenSees 2.5.0., as shown in Figure 5. Figure 6 shows the detail of the SC-CBF structure's column base. The key difference between SC-CBF and CBF structures lies in the unrestraint of the column base and setting prestressed tendon, so the stiffness of the GAP element plays a vital role here. The stiffness of the GAP element is 880×10^3 N/mm, the initial clearance is 0, and the critical force is 2×10^{10} N when the material reaches the plastic state. The default values in the OpenSees program are used for other parameters [16]. Steel 02 is adopted to simulate the steel, and beam column fiber element based on flexibility is selected; GAP element is selected for column base. The constitutive relation and axial deformation are shown in Figure 7, and the truss element is used for the simulation of the prestressed tendons.

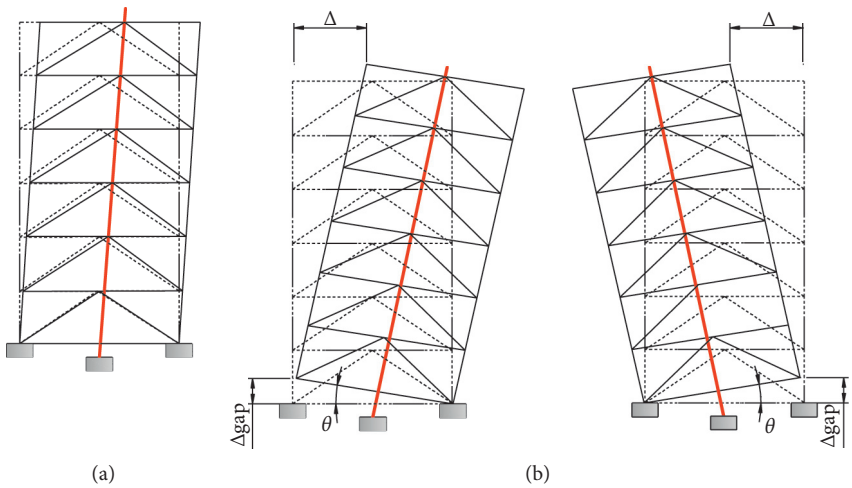

Figure 2: Rocking behavior of the SC-CBF structure.

Table 1: Sections of structure members.

Members	1st story	2nd story	3rd story	4th story
Beam	H400 × 250 × 12 × 18	H400 × 250 × 12 × 18	H400 × 250 × 12 × 15	H400 × 250 × 12 × 15
Column	H400 × 400 × 18 × 18	H400 × 400 × 18 × 18	H400 × 400 × 16 × 16	H400 × 400 × 16 × 16
Bracing	H250 × 250 × 10 × 15	H200 × 200 × 8 × 12	H200 × 200 × 12 × 15	H200 × 200 × 10 × 12

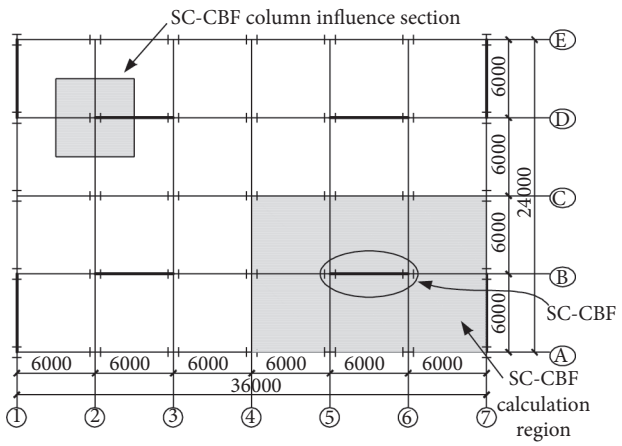

Figure 3: Floor plan of structure.

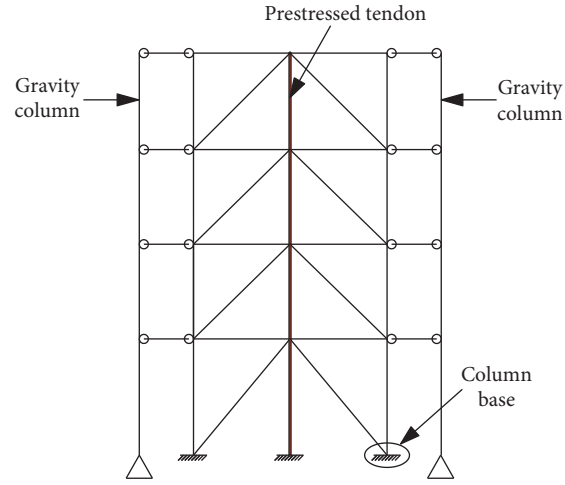

Figure 5: Model of the SC-CBF structure.

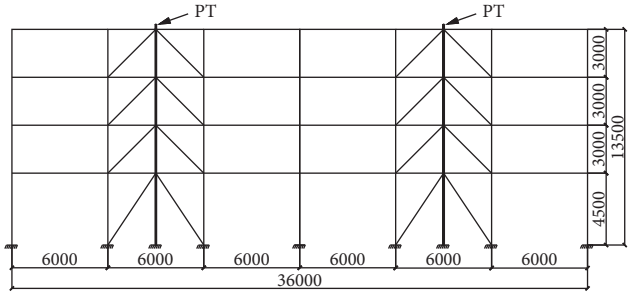

Figure 4: Elevation of the SC-CBF structure.

3. Nonlinear Analysis and Results

3.1. Pushover Analysis Results. The finite element model of the SC-CBF structure was established completely, and the corresponding pushover analysis was performed. The target displacement of the CBF structure is set to 270 mm (2%), while the SC-CBF structure has a large lateral deformation, so its target displacement is set as 540 mm (4%). The base shear-top displacement curves of two structures are shown in Figure 8.

It can be seen from Figure 8 that the two pushover curves have significant differences. On the one hand, the yield displacement of the two structures is quite different.

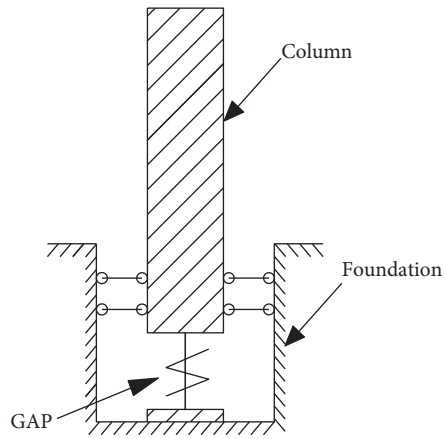

Figure 6: The detail of the SC-CBF structure's column base.

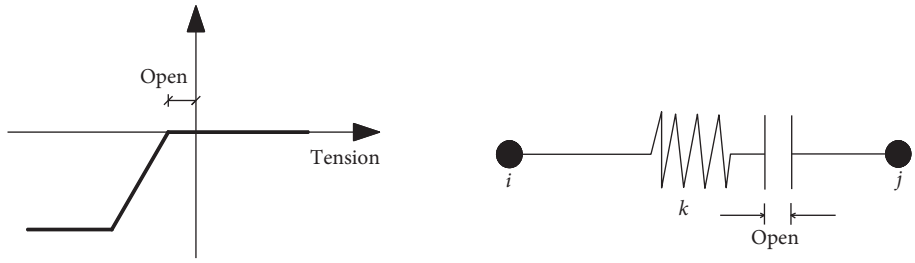

Figure 7: Constitutive relation and axial deformation of the GAP element.

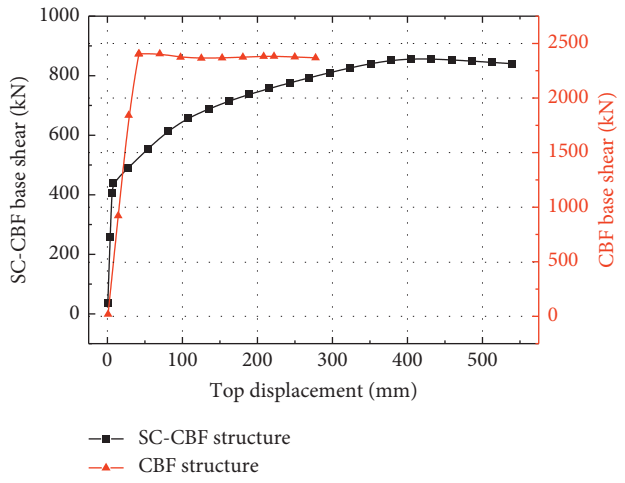

Figure 8: Pushover curves for SC-CBF and CBF structures.

The yield displacement of the SC-CBF structure is about 400 mm, while that of the CBF structure is only about 35 mm. Thus, SC-CBF has stronger lateral resistance than the CBF structure. On the other hand, the maximum base shear of the SC-CBF structure and CBF structure is about 800 kN and 2400 kN, respectively. The maximum base shear value of the CBF structure is almost three times that of the SC-CBF structure, which indicates that the CBF structure exhibits greater damage risk than the SC-CBF structure. Furthermore, the SC-CBF structure displays a better energy dissipating capacity due to that the structure becomes "flexible" by loosening the column base. However, the CBF structure has a larger rigidity and can bear more seismic force due to its fixed foundation.

Figure 9 shows the pushover curve for the SC-CBF structure. Figure 10 shows the curve between the axial force of prestressed tendons and top displacement. Figures 9 and 10 show the four limit states of the SC-CBF structure under the action of earthquake. The branches A to B, B to C, and C to D in Figure 10 correspond to the column base decompression and uplift stage, decompression and uplift stage to the yield stage of prestressed tendon, and the yield to failure stage of structural members, respectively, in Figure 9.

Figure 11 is the curve of uplift displacement versus top displacement of GAP. Figure 12 is the curve of force versus deformation of GAP. The direction of the applied load here is from left to right. As for GAP, the left GAP in the structure is tensioned and experiences the uplift displacement, as shown in Figure 11. Figure 12 shows the force of the GAP drops to zero after the column base is decompressed. The right GAP is in compression, and its stiffness is large; its displacement does not change. Meanwhile, the force of the right GAP element increases with the top displacement, but the force keeps constant after the prestressed tendon yields.

3.2. Low-Cycle Repeated Loading Analysis Results. The identical finite element model is adopted to perform the cyclic pushover analysis, and the same horizontal force and

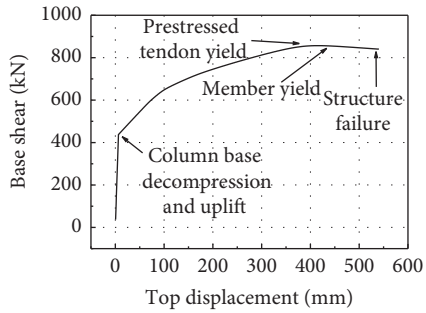

Figure 9: Pushover curve for the SC-CBF structure.

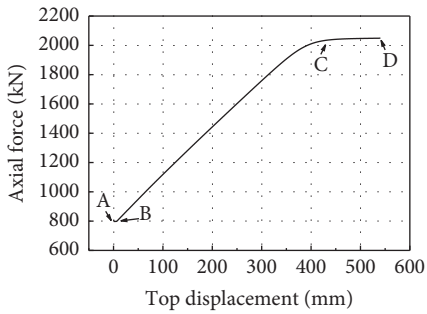

Figure 10: Curve between the axial force of the prestressed tendon and top displacement.

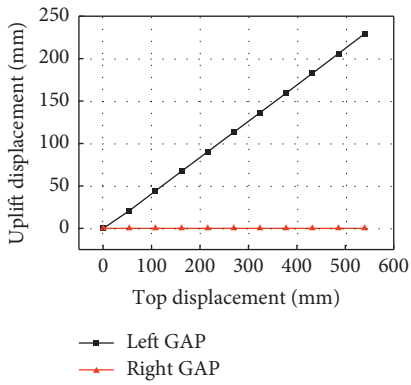

Figure 11: Uplift displacement versus top displacement of GAP.

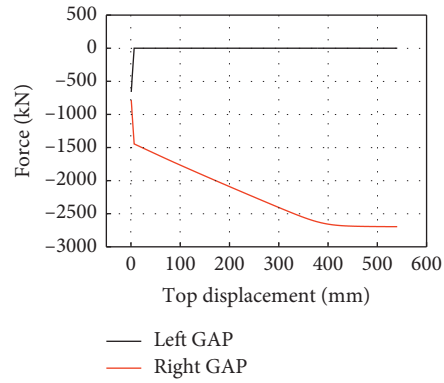

Figure 12: Force versus deformation of GAP.

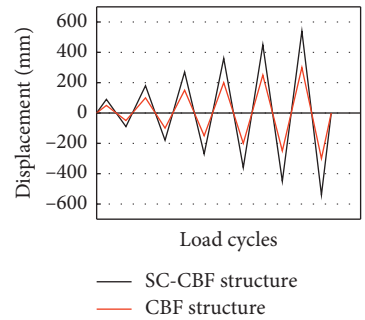

Figure 13: Cyclic loading protocol.

maximum displacement value were used for loading as monotonic pushover analysis. The cyclic loading protocol is shown in Figure 13.

Figure 14 compares the hysteresis loops of SC-CBF and CBF structures, respectively. It can be seen from the figure that the performance of two structures is significantly different under the action of low-cycle repeated loading. However, the hysteresis loop of the SC-CBF structure is a typical flag shape, which is basically consistent with the expectation. Before the top displacement of the structure reaches 400 mm and the structure displays a good lateral resisting ability, there is no obvious structural stiffness degradation. During the unloading, the deformation recovers quickly, and the residual drift of SC-CBF structure is close to zero, achieving the self-centering expectation smoothly. Meanwhile, good energy dissipation can be observed corresponding to the shuttle shape exhibited in the hysteresis loop of CBF structure, but the recovery of structural deformation is small when unloading, and there is a significant recovery of deformation hysteresis phenomenon. After that, the slope of the curve gradually decreases with the increase in load, which indicates the structure undergoes stiffness degradation obviously, while the structural residuals drift is large after unloading.

The prestressed tendons stress-top displacement curve of the SC-CBF structure during the cyclic loading are shown in Figure 15. However, the prestressed tendon has some losses of prestress before yielding of the prestressed tendon. However, the loss of prestress gradually increases with the increase in the top displacement after the prestressed tendon yields, and the increment is more significant especially when the structure's top displacement reaches 540 mm; the loss of prestress arrives at the largest, about 550 MPa. In this case, the prestressed tendon can be seen as ineffective, which is corresponding to the fortification goals of life safety under the rare earthquake.

It can be seen from Figure 16 that the base shear of the structure increases along with the uplift displacement of GAP. When the uplift displacement of GAP is removed, the base shear change in the structure is small, which is because the prestressed tendon always provides a vertical tensile force for structure. Furthermore, the stress of GAP in Figure 17 increases with the increase in the top displacement; it

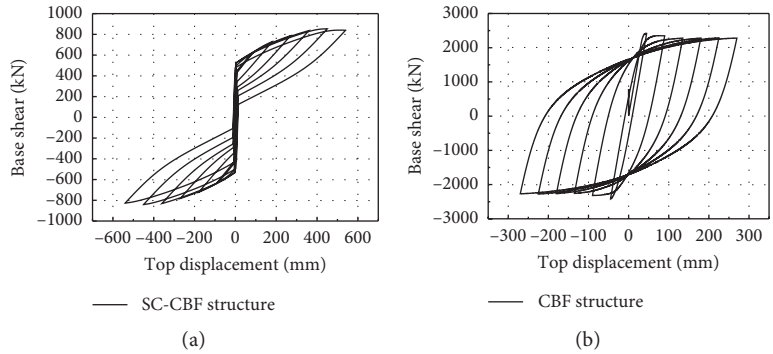

Figure 14: Hysteresis loops of structures.

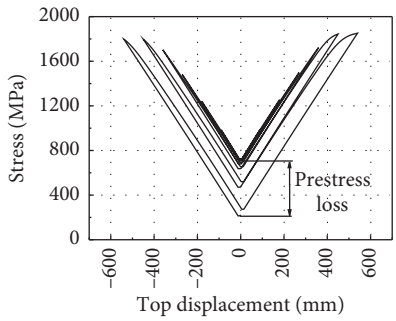

Figure 15: Curve of prestressed tendons stress versus top displacement.

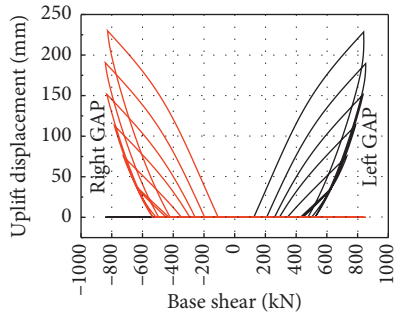

Figure 16: Curve of uplift displacement versus base shear of GAP.

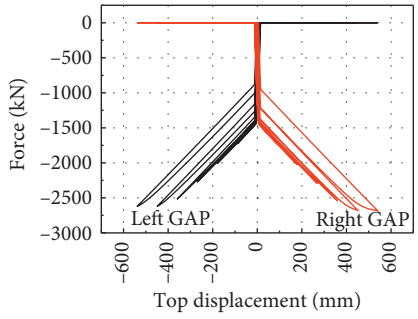

Figure 17: Curve of force versus top displacement of GAP.

suddenly increases when the top displacement starts to change, and then, the amplitude becomes smaller. When the top displacement of the structure reaches 400 mm, the force of GAP degenerates during unloading. This is caused by yields of the prestressed tendon, which leads to the change in the overall mechanical performance of the SC-CBF structure.

3.3. Elastoplastic Time-History Analysis Results. The elastoplastic time-history analysis has advantages in observing the whole seismic response process of the structure under the earthquake action, so the seismic response and self-centering performance analysis for SC-CBF and CBF under rare earthquake and extremely rare earthquake is performed by elastoplastic time-history analysis in OpenSees software. The peak value of the earthquake accelerograms in the time-history analysis is determined by the Chinese standard and code [5, 17]. The selected earthquake waves are El Centro wave, Taft wave, and artificial wave, and the design basis acceleration is 0.20 g. The peak accelerations are 0.40 g and 0.60 g corresponding to intensity 8 rare earthquake and extremely rare earthquake, respectively.

It can be seen from Figures 18 and 19 that the top displacement of the SC-CBF structure is nearly twice than that of the CBF structure. This is due to the unrestrained column base of the SC-CBF structure, reducing the rigidity of the structure, which provides a greater lateral drift under the earthquake forces. Owing to the prestressed tendon's tensile recovery effect, the SC-CBF structure's drift curves have more peak points than the CBF structure, as shown in Figure 19(b); SC-CBF structure has three peak drift points at 7 s, 14 s, and 24 s, which makes the top displacement of structure change greatly under the action of earthquake.

The peak interstory drift for the two structures is about 0.6% in Figure 20, which is less than the code's limit value of 2%. This is due to the large size of the frame selected in the calculation analysis here to fully study the recovery capacity of the prestressed tendon in SC-CBF, thus providing a great stiffness for the structure. At the same time, the structure can effectively meet strength requirements under the earthquake action. The interstory drift of the SC-CBF structure is larger than that of CBF, owing to the SC-CBF structure's small stiffness. However, it can be seen from Figure 21 that the residual drift of the SC-CBF structure is far smaller than that of CBF under different earthquake actions. In general, the good self-centering performance of the SC-CBF structure is fully demonstrated.

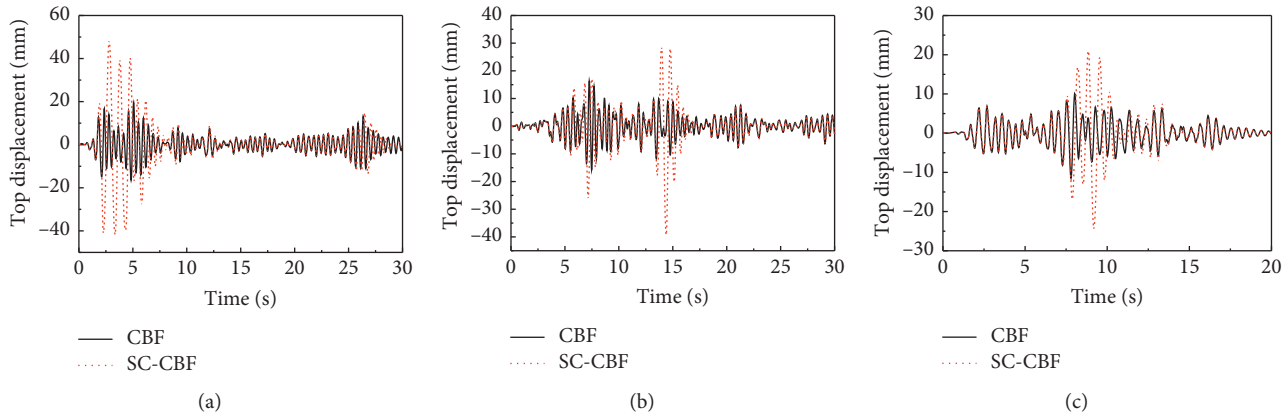

Figure 18: Top displacement versus time curves of the structure under rare earthquake: (a) El Centro wave; (b) Taft wave; (c) artificial wave.

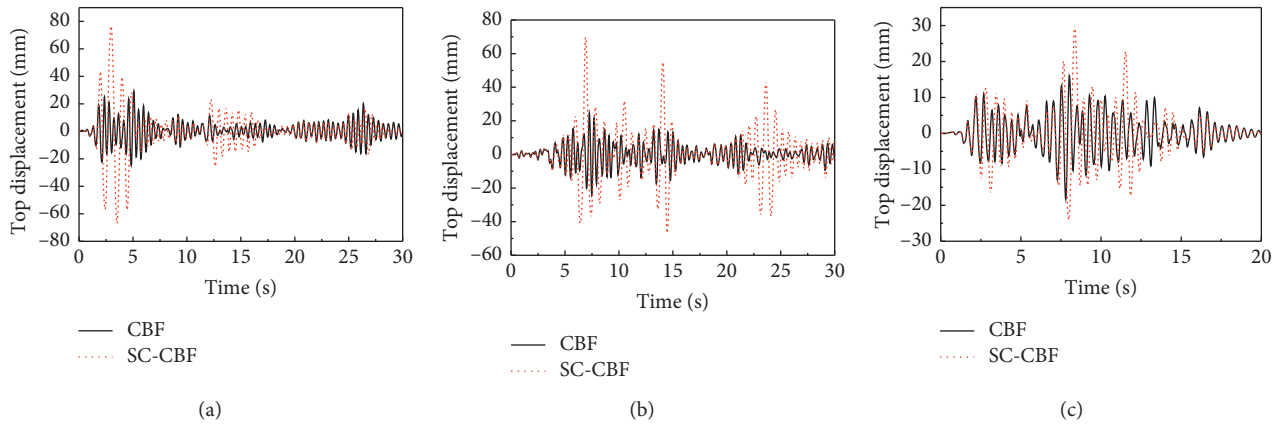

Figure 19: Top displacement versus time curves of the structure under extremely rare earthquake: (a) El Centro wave; (b) Taft wave; (c) artificial wave.

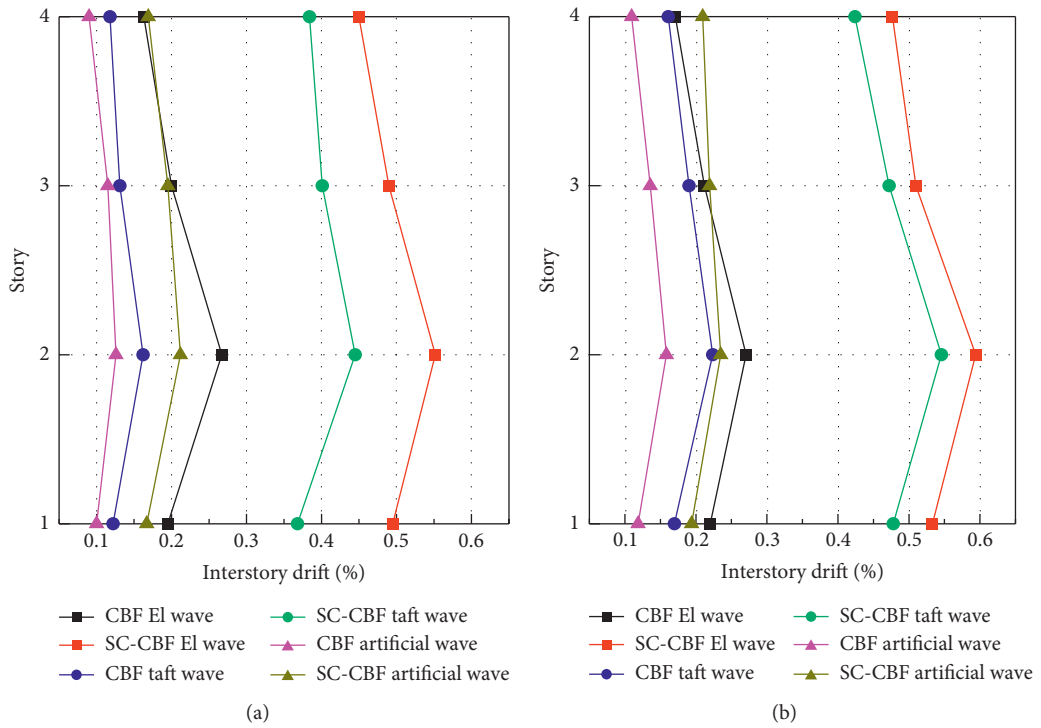

Figure 20: Peak interstory drift of 4-story structure under earthquake actions: (a) rare earthquake; (b) extremely rare earthquake.

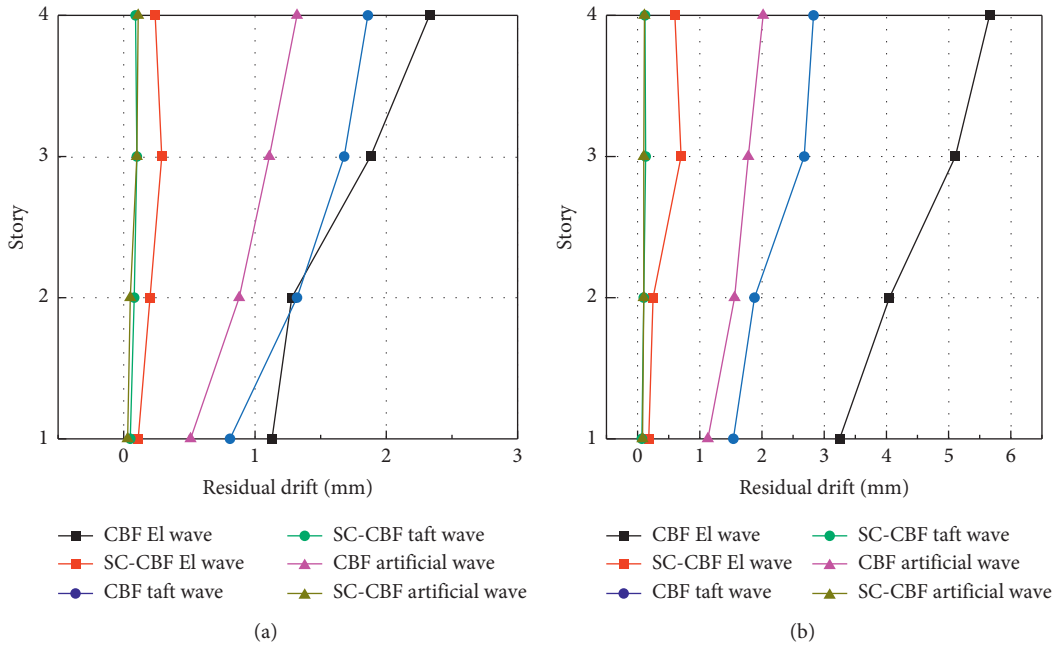

Figure 21: Residual drift response of 4-story structure under earthquake actions: (a) rare earthquake; (b) extremely rare earthquake.

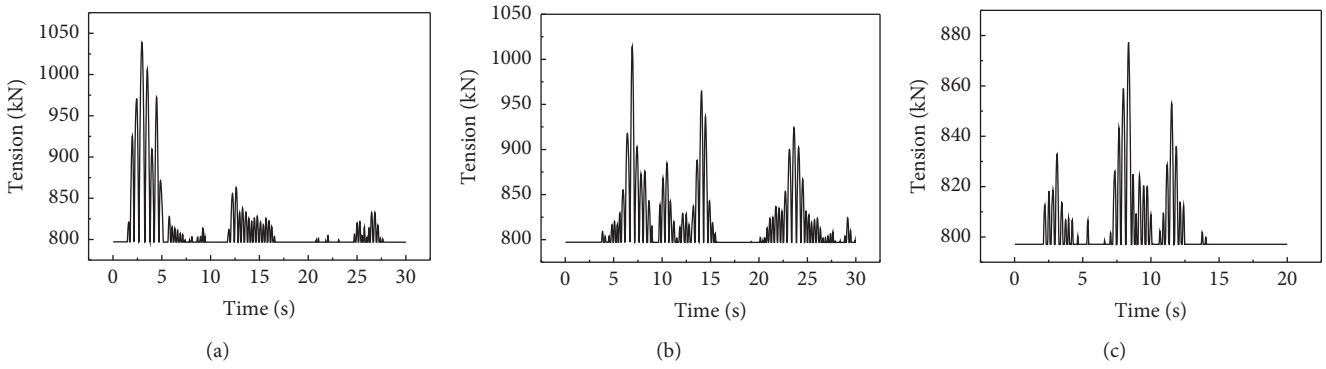

Figure 22: Axial tension time-history curves of prestressed tendons under extremely rare earthquake: (a) El Centro wave; (b) Taft wave; (c) artificial wave.

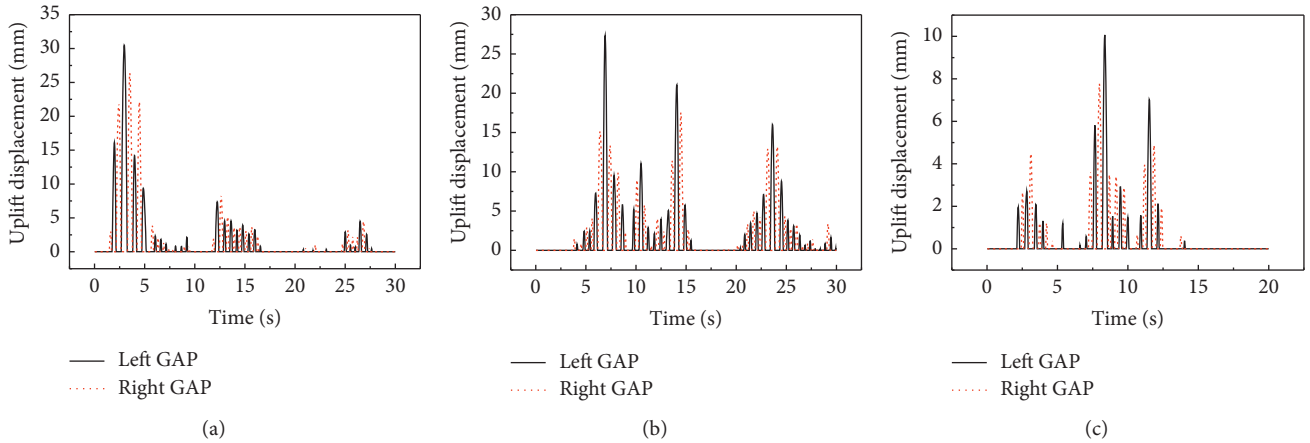

Figure 23: Time-history curves of GAP's uplift displacement under extremely rare earthquake: (a) El Centro wave; (b) Taft wave; (c) artificial wave.

The time-history analysis results of structures' members under extremely rare earthquakes are shown in Figures 22 and 23. Wherein, Figure 22 shows that the peak axial force of prestressed tendon reaches the maximum 1040 kN under earthquake, and the prestressed tendon does not yield in this case, which can provide a sufficient restoring force for the structure. In addition, it can be seen from Figure 23 that GAP element would experience a certain uplift displacement under earthquake, which provides a good rocking behavior and overall displacement ductility for the structure. The uplift displacement of the left GAP element is obviously larger than that of the right side, which is due to the earthquake waves inputted from left to right. After left-side GAP has undergone the earthquake, the SC-CBF structure has dissipated a certain amount of earthquake energy, and the right GAP's uplift displacement would decrease in this case. As the amplitude of GAP uplift displacement increases, the axial tension of prestressed tendon increases. Because the prestressed tendon does not yield all the time, SC-CBF structure exhibits a good seismic performance.

4. Parametric Analysis of SC-CBF Structure

The mechanical behavior of the SC-CBF structure under earthquakes is complicated. In order to understand the SC-CBF structure's self-centering characteristic and seismic performance comprehensively, it is necessary to analyze the structural performance under different design parameters. Thus, the stiffness of the GAP element and the cross-sectional area of prestressed tendon are selected for parameter analysis in this section, which is because the relaxation of column base and the application of prestressed tendon will significantly influence the structural performance.

4.1. Effect of Stiffness for GAP. To explore the influence of different GAP on the seismic performance of structure, the stiffness of the GAP was selected as K, $1/2K$, and $1/4K$, respectively, and the low-cycle repeated loading analysis was carried out here.

Figures 24 and 25 are the hysteresis loop of the base shear versus top displacement and its skeleton curve, respectively. Figure 24 manifests that three hysteresis loops become a typical flag shape, and the envelope of the loops is basically identical under different GAP stiffnesses, which verifies the good self-centering performance of the SC-CBF structure. It can be seen from Figure 25 that the slope of skeleton curve decreases along with the gradual decline in GAP stiffness until the decompression and uplift of column base. In addition, the GAP stiffness also has a great impact on the yield displacement. From Figure 25, the structures' top displacement with stiffness of K, $1/2K$, and $1/4K$ of GAP is 400 mm, 450 mm, and 520 mm, respectively, when structure yields, which can be explained from the stress change in the prestressed tendons.

The yield displacement of prestressed tendons has a significant difference under different GAP stiffnesses in Figure 26. The smaller the GAP stiffness is, the larger the yield displacement is, and the larger the lateral drift of the structure is, which also leads to the change in the yield point for the SC-CBF structure. The smaller the initial prestress of the prestressed tendons, the smaller the GAP stiffness in the initial mechanical phase. Although the same initial prestress has been defined in the analysis, the difference of the initial prestress would also exist due to the constitutive properties of GAP. When the stiffness of GAP is K, the prestressing

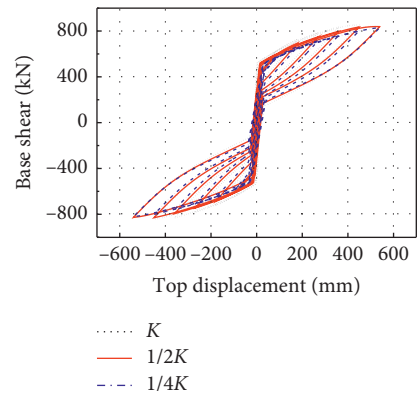

Figure 24: Hysteresis loop of the base shear versus top displacement.

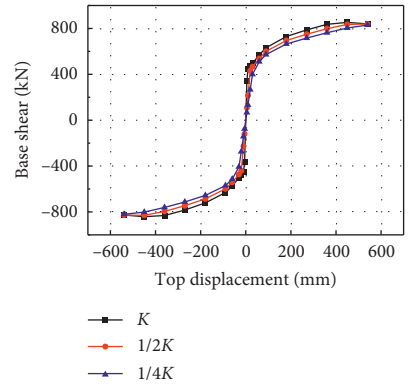

Figure 25: Skeleton curve.

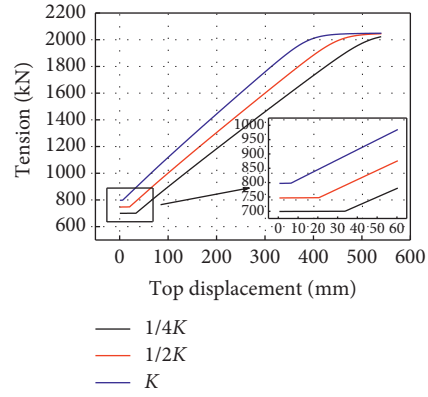

Figure 26: Prestressed tendon axial force-top displacement curve.

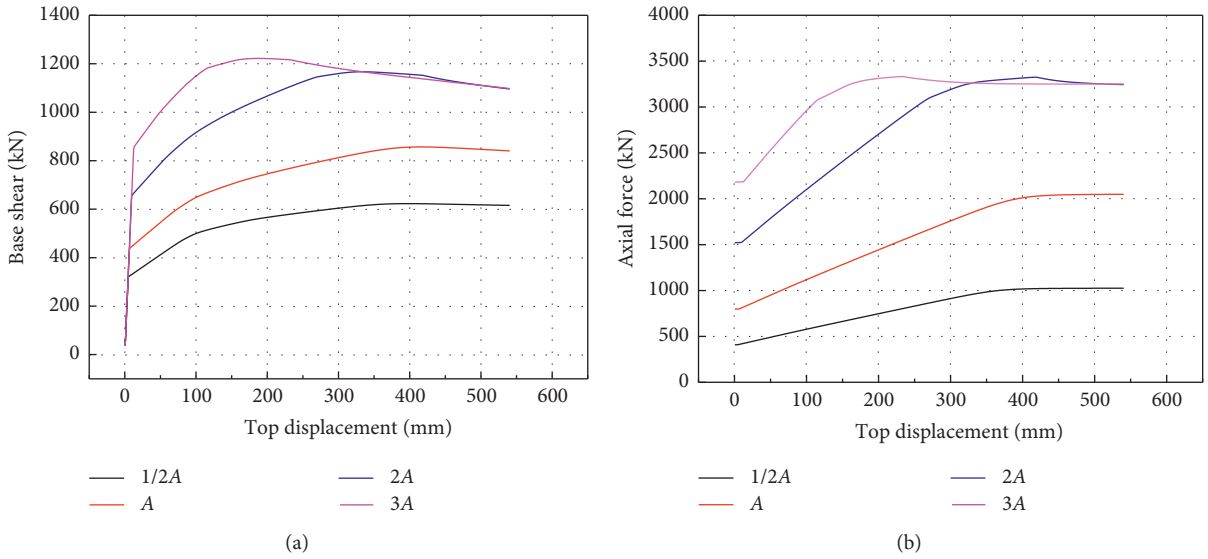

Figure 27: (a) Pushover curve of base shear versus top displacement; (b) pushover curve of axial force versus top displacement.

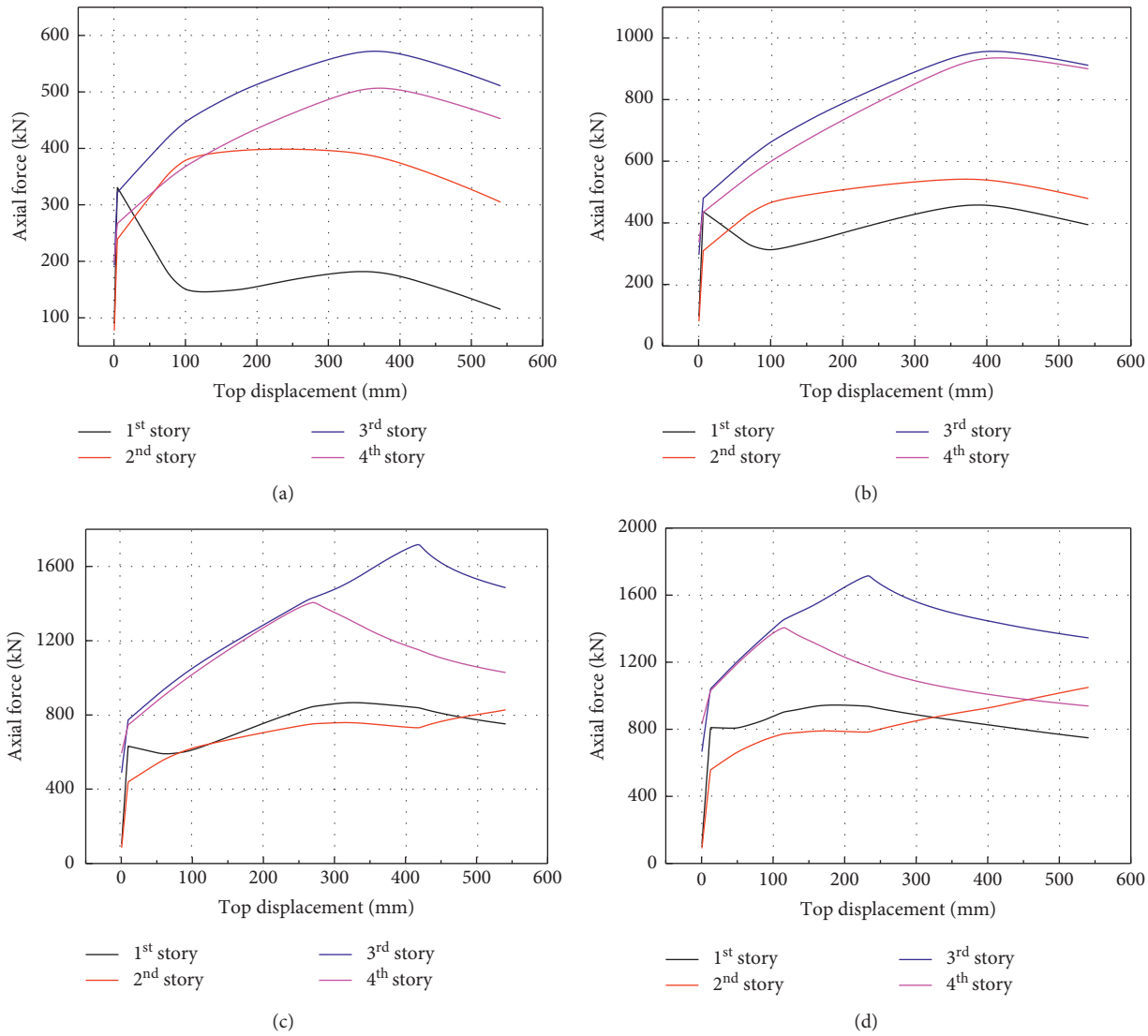

Figure 28: Pushover results of bracing axial force versus top displacement with different areas in each story: (a) 1/2*A*; (b) *A*; (c) 2*A*; (d) 3*A*.

force begins to increase when the top displacement is 6 mm, and then the prestressed tendon begins to extend; the corresponding displacement is 20 mm and 34 mm, respectively, when the stiffness is 1/2K and 1/4K.

4.2. Effect of the Prestressed Tendons Cross-Sectional Area. As we know, the prestressed tendon can provide self-centering force for the SC-CBF structure, but the performance would display some differences with variable cross-sectional tendon. The cross-sectional area for tendons were selected as A, 2A, and 3A, respectively, to analyze the seismic performance for the SC-CBF structure.

4.2.1. Pushover Analysis. Pushover analysis was performed here to study the influence of different sections of prestressed tendon on the limit state for the SC-CBF structure. Figure 27 exhibits the pushover results of base shear and axial force versus top displacement for different section areas of prestressed tendons, respectively. For different sections of the prestressed tendon, the curves of axial force-top displacement for bracings at each story are shown in Figure 28. In the illustration, A is the cross-sectional area of prestressed tendon.

In Figure 27(a), the pushover curve of the SC-CBF structure keeps the same tendency with the cross-sectional areas of 1/2A, A, and 2A, but the maximum base shear occurs at small yield displacement as the area is 3A. In case of the prestressed tendon cross-sectional area being less than 2A, the base shear of the structure increases gradually with the increase in the cross-sectional areas of the prestressed tendon, and there would exist an obvious difference in the maximum base shear. Nevertheless, the difference in maximum base shear is small when the cross-sectional area is between 2A and 3A, which indicates that the design of the prestressed tendons must fully consider the structural overall performance.

As is shown in Figure 27(b), the peak axial tensile force of prestressed tendon is about 1000 kN and 2000 kN, respectively, with tendons' cross-sectional areas of 1/2A and A, which has reached the yield point. Furthermore, when the structure is with 2A and 3A cross-sectional areas, the peak axial tension of prestressed tendon is about 3250 kN, and the prestressed tendon has not yielded in this case.

The influence of cross-sectional areas of prestressed tendons on the limit state of the structure can be analyzed according to the bracing's axial force reflected in Figure 28. It can be seen from Figures 28(a) and 28(b) that the force of bracings in each story is relatively small, and the bracing has not yielded before the prestressed tendons yield, which conforms to the ideal sequence of limit state for the SC-CBF structure. The bearing capacity of the structure reduces when the prestressed tendons yield, and the bearing capacity of the bracing decreases gradually. Therefore, the bracing's axial force decreases with the increase in the top displacement. In Figures 28(c) and 28(d), the third and fourth story bracings' forces are about 1700 kN and 1400 kN, and it has reached the value of yield now. The pushover results show a significant

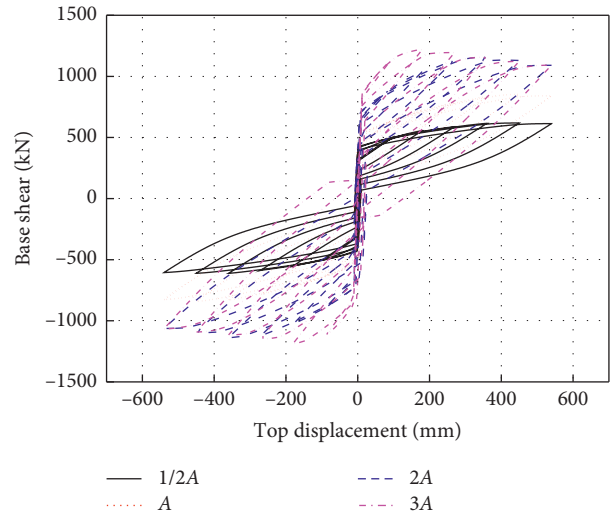

Figure 29: Hysteresis loop of base shear versus top displacement.

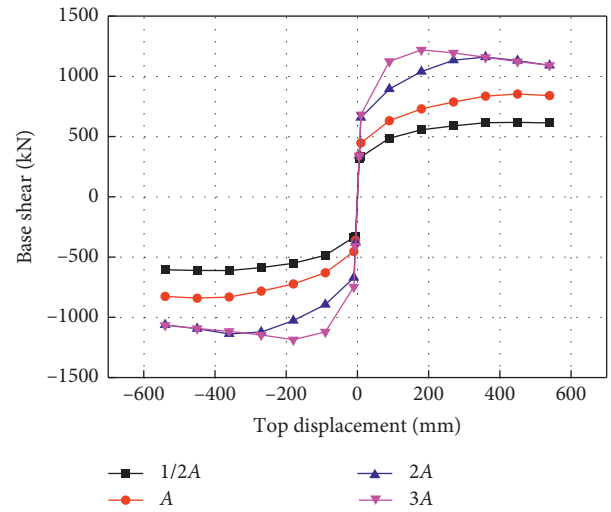

Figure 30: Skeleton curve.

decline tendency, which is different from the decline of bracing's axial force in Figures 28(a) and 28(b). At the yield of the third and fourth story bracings, the prestressing force of the prestressed tendon also decreases gradually, leading to the sequence changes in the limit state of the SC-CBF structure, and the members yield after the column base decompresses and uplifts, which cannot meet the requirements of the performance-based design method.

4.2.2. Low-Cycle Repeated Loading Analysis. To explore the seismic and energy dissipating performance of the SC-CBF structure with different cross-sectional areas of prestressed tendon, the low-cycle repeated loading analysis was carried out in this section. Figures 29 and 30 are the hysteresis loop of the base shear versus top displacement and its skeleton

curve for four different tendon's cross-sectional areas, respectively.

The prestressed tendons would provide the restoring force for the structure, and it does not change with the difference in tendons' cross-sectional areas. The hysteresis loop presents a flag shape, and the envelope area of the loop increases along with the increase in the tendons' cross-sectional areas, indicating that the ability of energy dissipation is significantly affected by the cross-sectional areas. However, the structure has a large residual drift when the cross-sectional area is 3A in case of the yielding of the bracings. The bracing's yield induces the improvement in the energy dissipation, but the members undergo an unrecoverable plastic deformation after unloading. Figure 30 shows that the structure's base shear increases with the increasing areas of tendons, and the displacement increases during the column decompression. Moreover, the decline of base shear becomes more obvious just as the base shear reaches the peak value, and the structure stiffness decreases greatly during reloading and unloading. Especially, when the cross-sectional area is 3A, the stiffness decreases most significantly.

5. Conclusion

In this paper, through the OpenSees program, the mechanical and seismic performances are researched for the SC-CBF and CBF structures by the static elastoplastic analysis, low-cycle repeated loading analysis, and elastoplastic time-history analysis. Some conclusions can be drawn from the results of this investigation:

(1) Pushover analysis results of the SC-CBF structure verify its mechanical properties and four-stage limit states. SC-CBF structure has a stronger lateral resistance capacity, a small base shear, and a good displacement ductility under earthquake action, compared with the CBF structure, which can ensure the structure safety effectively.

(2) The hysteresis loop of the SC-CBF structure presents a flag shape with a prominent self-centering performance. The residual drift of the structure is small, and the prestress loss is small when the prestressed tendon is unloaded before yielding. However, the CBF structure hysteresis loop is full of "Shuttle," displaying a good energy dissipation, but the residual drift is large when unloading, and the stiffness degradation phenomenon is obvious.

(3) Under the rare and extremely rare earthquakes, the SC-CBF structure experiences a larger drift response, the maximum interstory drift is about 2-3 times than that of CBF structure, but the residual drift when unloading is just 1/10 of CBF structure according to the elastoplastic time-history analysis result, which fully reflects its good ductility and self-centering performance.

(4) When the stiffness of GAP decreases by 1/2 and 3/4, the top displacement increases for 12.5% and 30%, and the structural lateral drift increases meanwhile. With the decrease in GAP stiffness, the initial stress of prestressed tendon decreases, but the yield displacement of prestressed tendon increases.

(5) The base shear and the axial force of the prestressed tendon increase with the increase in the sectional areas of the prestressed tendons, the hysteresis loop becomes full, and the energy dissipation capacity is increased with the change in areas. When the increment of the cross-sectional areas arrives to a certain extent, the failure mechanism of the SC-CBF structure would change, which is because the prestressed tendons have not yet yielded when the components yield, so the overall performance of the structure must be considered when designing the prestressed tendons for the structure.

Data Availability

The data used to support the study can be available upon request to the corresponding author.

Conflicts of Interest

The authors declare that there are no conflicts of interest regarding the publication of this paper.

Acknowledgments

This research was funded by the National Natural Science Foundation of China (Grant nos. 51808046 and 51108035), Natural Science Basic Research Plan in Shaanxi Province of China (Grant nos. 2020JQ-917, 2017JQ5061, 2016JM5007, and 2013JM7030), Special Fund for Basic Scientific Research of Central College (Grant nos. 310828162017, 310828161009, and 310841171001), and Scientific Research Fund of Xi'an Eurasia University (Grant no. 2018XJZK03).

References

[1] A. Dall'Asta, G. Leoni, F. Morelli, W. Salvatore, and A. Zona, "An innovative seismic-resistant steel frame with reinforced concrete infill walls," *Engineering Structures*, vol. 141, pp. 144–158, 2017.

[2] Y. Li, R. Song, and D. L. J. W. Van, "Collapse fragility of steel structures subjected to earthquake mainshock-aftershock sequences," *Journal of Structural Engineering*, vol. 140, no. 12, Article ID 04014095, 2014.

[3] China Architecture and Building Press, *Code for Seismic Design of Buildings: GB 50011-2010*, China Architecture and Building Press, Beijing, China, 2010, in Chinese.

[4] M. Bruneau, S. E. Chang, R. T. Eguchi et al., "A framework to quantitatively assess and enhance the seismic resilience of communities," *Earthquake Spectra*, vol. 19, no. 4, pp. 733–752, 2003.

[5] Resilient City Report, *Defining What San Francisco Needs from its Seismic Mitigation Policies*, The San Francisco Planning and Urban Research Association, San Francisco, CA, USA, 2009.

[6] M. Grigorian, A. S. Moghadam, H. Mohammadi, and M. Kamizi, "Methodology for developing earthquake-resilient structures," *The Structural Design of Tall and Special Buildings*, vol. 28, no. 2, Article ID e1571, 2019.

[7] C. C. Chou and J. H. Chen, "Development of post-tensioned self-centering structures for earthquake resistance," *International Journal of Structural Engineering*, vol. 3, no. 1-2, pp. 1–17, 2012.
[8] A. Hassanzadeh and S. Gholizadeh, "Collapse-performance-aided design optimization of steel concentrically braced frames," *Engineering Structures*, vol. 197, Article ID 109411, 2019.
[9] J. M. Ricles, R. Sause, M. M. Garlock, and C. Zhao, "Post-tensioned seismic-resistant connections for steel frames," *Journal of Structural Engineering*, vol. 127, no. 2, pp. 113–121, 2001.
[10] D. Roke, R. Sause, J. M. Ricles, C. Y. Seo, and K. S. Lee, "Self-centering seismic-resistant steel concentrically-braced frames," in *Proceedings of 5th International Conference on Behaviour of Steel Structures in Seismic Areas*, pp. 85–90, Yokohama, Japan, 2006.
[11] R. Sause, J. M. Ricles, Y. C. Lin, C. Y. Seo, D. Roke, and N. B. Chancellor, "Self-centering damage-free seismic-resistant steel systems," in *Proceedings of 7CUEE & 5ICEE*, pp. 39–48, Tokyo, Japan, 2010.
[12] D. Roke, R. Sause, J. M. Ricles, and N. Goner, "Design concepts for damage-free seismic-resistant self-centering steel concentrically-braced frames," in *Proceedings of 2009 ASCE Structures Congress*, pp. 1–10, Reston, VA, USA, 2009.
[13] R. Sause, J. M. Ricles, D. Roke, N. B. Chancellor, and N. Goner, "Large-scale experimental studies of damage-free self-centering concentrically-braced frame under seismic loading," in *Proceedings of 2010 ASCE Structures Congress*, pp. 1495–1509, Reston, VA, USA, 2010.
[14] China Architecture and Building Press, *Load Code for the Design of Building Structures: GB 50009-2012*, China Architecture and Building Press, Beijing, China, 2012, in Chinese.
[15] L. W. Yang, *Seismic Performance Analysis of Self-Centering Steel Concentrically Braced Frames Based on OpenSees. Master Dissertation*, Chang'an University, Xi'an, China, 2018, in Chinese.
[16] D. Roke, *Damage-free seismic-resistant self-centering concentrically-braced frames*, Ph.D. thesis, Lehigh University, Bethlehem, PA, USA, 2010.
[17] Standards Press of China, *Seismic Ground Motion Parameter Zonation Map of China: GB 18306-2015*, Standards Press of China, Beijing, China, 2015, in Chinese.